Nonlinear optical properties of Langmuir-Blodgett monolayers

Cnossen, Gerard; Drabe, Karel E.; Wiersma, Douwe A.

Published in:
The Journal of Chemical Physics

DOI:
10.1063/1.463895

Nonlinear optical properties of Langmuir–Blodgett monolayers: Local-field effects

Gerard Cnossen, Karel E. Drabe, and Douwe A. Wiersma
University of Groningen, Materials Science Center, Ultrafast Laser and Spectroscopy Laboratory, Nijenborgh 4, 9747 AG Groningen, The Netherlands

(Received 2 April 1992; accepted 8 June 1992)

Detailed measurements of the macroscopic second-order optical nonlinearity $\chi^{(2)}(2\omega,\omega,\omega)$ of Langmuir–Blodgett dye-doped monolayers are reported. The observed deviations from a linear behavior of $\chi^{(2)}$ with increasing surface density are shown to be due to local-field effects. In order to calculate these local-field factors for disordered systems, a novel Monte Carlo type calculation is introduced. This calculation not only accounts for density variations in the monolayers but also incorporates the effect of off-diagonal elements of the (microscopic) linear susceptibility tensor. Quantitative agreement is found between the calculations and the experimental results using only the molecular hyperpolarizability as a free parameter. A method is presented to determine the tilt angle of the chromophores in Langmuir–Blodgett monolayers from the anisotropy of the linear absorption. The tilt angle determined this way is in excellent agreement with a determination by second-harmonic generation.

I. INTRODUCTION

Second-harmonic generation has become one of the most important optical techniques to study the properties of monolayers and interfaces.[1] Due to its great sensitivity to breaking of inversion symmetry, information can be obtained about the structure and ordering of molecules at interfaces.

In order to evaluate the second-harmonic intensity in terms of the structure and ordering of the optically nonlinear molecules, the geometry of the sample is important. The sample can be considered to be build up of three distinct media, namely the substrate, the optically active monolayer, and the superstrate. Each medium has its own dielectric constant. At the interface between the different media, an optical beam undergoes reflection and refraction resulting in a change of the electromagnetic field intensity. This change in local field is often described in terms of *geometric* (or macroscopic) local-field factors.[2–5] The geometric local-field factors can be found by solving the macroscopic Maxwell equations when the correct boundary conditions are employed.

A clear manifestation of the geometric local field appears in the case of Raman scattering and second-harmonic generation at rough surfaces. Signal enhancement is found due to field resonances in the protrusions at the surface,[3–5] and the correct long-range-distance dependence is predicted.[6,7] In case of smooth surfaces the macroscopic local field manifests itself in the form of a modulated fluorescence spectrum of a 1 μm thick layer of emitting dye molecules in front of a mirror.[8,9] The modulation pattern in the emission spectrum can be explained in terms of frequency dependent (geometric) local-field factors. Another example of a local-field effect is the enhancement by a factor of 3 to 10 of the signal strength that is observed at the critical angle in an internal reflection experiment.[2] These effects are evident in fluorescence[10] and frequency doubling[11] experiments.

In addition to the geometric local-field factors one has to consider the microscopic local field caused by dipolar interactions between the molecules. This *microscopic* local field is much more difficult to handle, because a good knowledge of the system on a molecular level is required. The calculation of this field in a two-dimensional lattice of rigid molecules is the subject of this paper.

By introducing microscopic local-field factors, the calculation of the response of an interacting ensemble of molecules to an electromagnetic field is reduced to a calculation of the response of isolated molecules interacting with the local field.[12] At optical frequencies Lorentz–Lorenz type of expressions[13] are often used to describe the microscopic local field. These expressions are valid for three-dimensional isotropic or cubic media.[13]

The adequacy of the Lorentz–Lorenz expressions has been tested for liquids by Levine *et al.*[14] using static field-induced second-harmonic generation. Good agreement between theory and experiment was found. The Lorentz local-field approach was recently also shown to describe the resonant linear and nonlinear optical response of a dense potassium vapor.[15]

In ordered systems of lower dimension like molecular aggregates and Langmuir–Blodgett monolayers, the Lorentz–Lorenz local-field expressions are not expected to be valid, and explicit numerical calculations involving all molecules need to be performed. However, because of its simplicity,[16,17] the Lorentz local-field expression is still often used for Langmuir–Blodgett monolayers. This approximation, however, may fail in case the optical excitations in the film are delocalized. In such cases it is the excitonic rather than molecular nonlinearity that should be accounted for and it has been shown by Spano *et al.*[18,19] that a local-field approximation breaks down.

In this paper we will study the applicability of the

 0021-9606/92/184512-13$006.00

local-field concept to a monolayer of dye molecules packed in a two-dimensional lattice. The Langmuir–Blodgett technique provides a way to systematically study the change in local field as a function of distance between the interacting chromophores. By mixing the optically active molecules with optically inactive ones it is possible to change the distance between the induced dipoles. By applying different surface pressures or by using different types of molecules it is also possible to change the mutual orientation between the interacting dipoles. In this way the intermediate regime between isolated molecular dipoles and the extended exciton state can be studied.

In this paper we report on the efficiency of frequency doubling of Langmuir–Blodgett monolayers as a function of concentration of the optically active molecules. In order to obtain a specific surface density these dye molecules are mixed with known amounts of inactive fatty-acid molecules.

Recently, several papers have reported on measurements of the second harmonic efficiency as a function of surface density.[20–30] The most popular system is a mixture of a hemicyanine dye and a fatty acid, which, however, is also known for its tendency to form aggregates at higher dye concentrations. Evidence for this aggregation effect is found in the spectrum of this molecule that undergoes a blueshift at high concentration.[21–25]

In these systems the second-harmonic efficiency decreases at dye concentrations higher than about 50 mole %.[20–28] Hayden[20] interprets this decrease solely in terms of the classical microscopic local-field factors as derived by Bagchi *et al.*[31,32] Absorption spectra were not reported by Hayden,[20] so it is difficult to judge whether aggregation plays a role in the samples used. Furthermore, details about the tilt angle of the dye unit are not provided, so the orientation between the optical dipoles is unknown. In addition, the interaction between the molecules is supposed to be independent of the mutual orientations of the dipoles.[20–23]

A number of groups have attributed the decrease of the second-harmonic intensity at high surface densities, to the centrosymmetric structure of the aggregate,[27,28] or to the dispersive effect of aggregation on the nonlinear susceptibility; the blueshift of the spectrum leads to a decrease of the resonance enhancement.[24,25] Others have described this decrease to a combination of aggregation and the classical microscopic local-field effect.[21–23]

It is obvious that aggregation in monolayers complicates the interpretation of frequency doubling experiments. The optically nonlinear systems dealt with in this paper show no signature of aggregation and are optically well characterized. This enables us to interpret the second-harmonic generation (SHG) efficiency in terms of microscopic local-field factors. The SHG efficiency is studied as a function of surface density for two different dyes. In one system the molecules are oriented almost parallel to the substrate, in the other system the dye attains a more erect position. In Sec. II we present a calculation of the microscopic local field by summing the near field of the surrounding dipoles in an iterative way, using a Monte Carlo type procedure. The orientation of the rodlike dye molecules is explicitly incorporated in the calculations. The off-diagonal components of the linear susceptibility tensor are also taken into account. In Sec. III the experimental details are reported. In Sec. IV we compare the results of calculations with the experimental results on SHG. Finally, in Sec. V we draw some conclusions.

II. THEORY AND NUMERICAL CALCULATIONS

A. General aspects

In adopting a theoretical framework for the calculation of the local field in Langmuir–Blodgett monolayers we make, as stated in the introduction, a distinction between geometrical and microscopic local-field corrections.[2–5]

The *geometrical* or macroscopic local-field correction factors relate the field components of the applied field to the corresponding ones in the monolayer and correct for the reflection and refraction of light. These factors are obtained by solving the Maxwell equations, applying the right boundary conditions.[2,5]

For later use we list here the expressions for the geometrical local-field correction factors for a monolayer on a flat substrate,[2–5]

$$L_{xx}=\frac{2\epsilon_1 k_{2z}}{\epsilon_2 k_{1z}+\epsilon_1 k_{2z}}, \tag{1a}$$

$$L_{yy}=\frac{2k_{1z}}{k_{1z}+k_{2z}}, \tag{1b}$$

$$L_{zz}=\frac{2\epsilon_1 k_{1z}(\epsilon_2/\epsilon')}{\epsilon_2 k_{1z}+\epsilon_1 k_{2z}}. \tag{1c}$$

Here x,y,z are the Cartesian laboratory coordinates as shown in Fig. 1. The z axis is normal to the substrate surface, while the y axis is normal to the plane of incidence. In this particular coordinate system the other components L_{ij} of the geometrical local-field tensor are zero. $\mathbf{k}_1(\mathbf{k}_2)$ is the wave vector for the field in medium 1(2), while $k_{1z}(k_{2z})$ is the projection of $\mathbf{k}_1(\mathbf{k}_2)$ onto the z axis. The dielectric constant of medium 1 (the superstrate) is denoted by ϵ_1, that of medium 2 (the substrate) by ϵ_2, and that of the monolayer by ϵ'. Note that these geometrical local-field factors are dependent on, (a) the choice of the substrate through ϵ_2, (b) the angle of incidence (through the projection of $\mathbf{k}_1$, $\mathbf{k}_2$ onto the z axis), and (c) the concentration of the dye molecules in the monolayer (through ϵ').

The *microscopic* local field is a manifestation of the reaction field of the induced dipoles within the monolayer. The local field along i $(i=x,y,z)$ at site n, denoted as $E^n_{\mathrm{loc},i}$, is calculated from[31–35]

$$E^n_{\mathrm{loc},i}=L_{ii}E_{0,i}+\sum_{m\neq n} E^m_{\mathrm{dip},i}. \tag{2}$$

Here $E_{0,i}$ is the externally applied field along i, and L_{ii} the geometrical correction factor given by Eq. (1). The dipolar field $\Sigma_{m\neq n}E^m_{\mathrm{dip},i}$ in the above equation is the reaction field of the surrounding dipoles, and is calculated from[13]

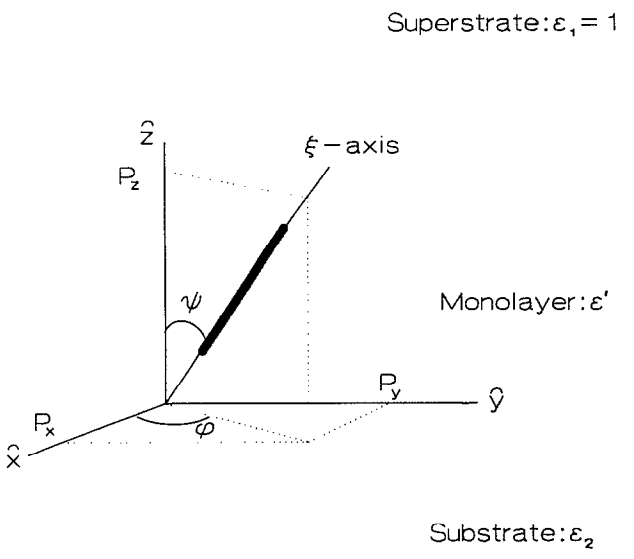

FIG. 1. Model system used in the calculations. The substrate surface is denoted by the $\hat{x}-\hat{y}$ plane. The z axis is normal to the substrate plane. The tilt angle ψ of the long axis of the dye unit (ξ axis) is assumed to have a site independent fixed value. In the isotropic monolayer case the projection angle ϕ is random at every site. In the crystal model ϕ has a fixed value.

$$\mathbf{E}^m_{\rm dip}(\mathbf{r}_n)=\frac{3\mathbf{n}(\mathbf{p}^m\cdot\mathbf{n})-\mathbf{p}^m}{|\mathbf{r}_{nm}|^3}. \tag{3}$$

Here $\mathbf{E}^m_{\rm dip}(\mathbf{r}_n)$ is the dipole field at site n due to an induced dipole $\mathbf{p}^m$ at site m. In Eq. (3) the unit vector $\mathbf{n}$ points from $\mathbf{r}_m$ to $\mathbf{r}_n$, and $|\mathbf{r}_{nm}|$ is the distance between sites m and n. The oscillating part of the electric field has not been incorporated in Eq. (3). In this near-field approximation the magnetic part of the electromagnetic field can be ignored.[13] Retardation effects have also been discarded. This assumption is justified by the calculations (Sec. II C), where the requirement $\mathbf{k}\cdot\mathbf{r}\ll 1$ is met.

The microscopic induced dipole moment $\mathbf{p}^m$ in Eq. (3) is related to the electromagnetic field by

$$\mathbf{p}^m=\mathbf{R}\boldsymbol{\alpha}\mathbf{R}^{-1}\mathbf{E}^m_{\rm loc}, \tag{4}$$

where $\mathbf{E}^m_{\rm loc}$ is the local electromagnetic field at site m, $\boldsymbol{\alpha}$ the linear molecular polarizability tensor, and $\mathbf{R}$ the rotation matrix connecting the molecular coordinate system to the laboratory frame. The local field is supposed to be uniform over the dimensions of the dipole (point–dipole approximation).

Note that we assume the induced dipole moment $\mathbf{p}^m$ to be determined entirely by the linear polarizability tensor $\boldsymbol{\alpha}$. The dominant component of the linear polarizability as well as the hyperpolarizability for the axially symmetric molecules studied is directed along the ξ axis (Fig. 1). Therefore, to an appreciable degree of accuracy the components of $\boldsymbol{\alpha}$ in the molecule-fixed axes system is

$$\boldsymbol{\alpha}=\begin{pmatrix}0 & & \\ & 0 & \\ & & \alpha_{\xi\xi}\end{pmatrix}. \tag{5}$$

Usually the other components of $\boldsymbol{\alpha}$ are an order of magnitude smaller for the molecules studied in this work.[36] The linear microscopic polarizability in the laboratory frame, however, is obtained by a similarity transformation $\mathbf{R}\boldsymbol{\alpha}\mathbf{R}^{-1}$, and is in general nondiagonal. The off-diagonal components of the microscopic linear polarizability are projections of $\alpha_{\xi\xi}$ on the different Cartesian axis (see Sec. II C).

It has been shown that for *any* polarizability the local field at a particular site can be obtained by inversion of the matrix form of Eq. (2).[37] This procedure, however, becomes impractical for large dipole lattices (>1000 dipoles) and is not always necessary either. In order to obtain the sum $\Sigma_{m\neq n}E^m_{{\rm dip},i}$ in Eq. (2), we follow an iterative procedure. In the first iteration the applied field $\mathbf{LE}_0$ is used to calculate the induced dipole moments $\mathbf{p}^m$. The local-field components at site n can now be calculated and are the sum of the applied field $L_{ii}E_{0,i}$ and the total reaction field of the surrounding dipoles $\Sigma_{m\neq n}E^m_{{\rm dip},i}$. In the second iteration the values obtained for the local-field components $E^n_{{\rm loc},i}$ are used to recalculate the induced dipole moment $\mathbf{p}^m$ and the accompanying reaction field.[34,38,39] As long as the amplitude of the total reaction field at site $\mathbf{r}_n$ remains smaller than the applied field, the successive orders ultimately converge to a constant value. If this is not the case then we have to invert the matrix form of Eq. (2) to obtain the local field. In order to calculate the successive orders both the orientation of and the distances to the neighboring molecules are needed.

Prior to presenting our results we will first provide, as a reference point, the results obtained from a crystal-like model. Thereafter we will present the results of a Monte Carlo calculation. The results of both models for the local field will be compared in Sec. II D.

B. The crystal model

In the crystal model all dipoles are placed equidistantly on a lattice and are assumed to have the same fixed orientation. For this case an analytical expression can be obtained for the sum of the reaction field of the surrounding dipoles $\Sigma_{m\neq n}E^m_{{\rm dip},i}$. The summation in Eq. (2) has been carried out by Topping,[40] and was used by Bagchi *et al.*[31,32] to calculate the dipole reaction field in a monolayer. The results for the microscopic local-field correction factors ℓ_{ii} are

$$\ell_{zz}=1/(1-\zeta_0\alpha_{zz}/a^3), \tag{6a}$$

$$\ell_{xx}=\ell_{yy}=1/(1+\zeta_0\alpha_{xx}/2a^3), \tag{6b}$$

where $\zeta_0=-9.0336\ldots$.[40] In these calculations the microscopic polarizability in the laboratory frame $\mathbf{R}\boldsymbol{\alpha}\mathbf{R}^{-1}$ was assumed to be diagonal. The image-dipole contribution from the glass substrate is omitted in Eq. (6) as it is assumed to be negligible.[35]

With the local-field correction factors given above, one obtains for the second-harmonic field components generated in the monolayer

$$E_i(2\omega) = AL_{ii}(2\omega)\ell_{ii}(2\omega)\chi^{(2)}_{ijk}(2\omega,\omega,\omega)L_{jj}(\omega)$$
$$\times \ell_{jj}(\omega)E_{0,j}(\omega)L_{kk}(\omega)\ell_{kk}(\omega)E_{0,k}(\omega). \quad (7)$$

Here L_{xx} is a geometrical factor given by Eq. (1), ℓ_{xx} is a microscopic local-field correction factor as given by Eq. (6), and $E_{0,j}$ is the externally applied field along j. Each local-field correction factor needs to be evaluated at the appropriate frequency. $\chi^{(2)}$ is the macroscopic second-order nonlinear susceptibility, and A is a proportionality factor, containing the direction and distance dependence of the emitted field $E_i(2\omega)$.

C. The isotropic monolayer model

For a numerical evaluation of the dipolar sum in Eq. (2) we need information concerning the orientation of the dipoles in the monolayer. This input is provided by a well-known model for a homogeneous Langmuir–Blodgett monolayer of rodlike molecules.[41] In this model, shown in Fig. 1, the long axis of the dye units are assumed to have the same tilt angle ψ with respect to the surface normal $\hat{z}$, but random projection angles ϕ onto the substrate plane $\hat{x}-\hat{y}$. In the density regime studied no correlations are supposed to exist between the orientations of neighboring dye units. In the molecular frame of the dye units, the *dominant* linear and second-order tensor components are assumed to be oriented along the ξ axis.

The long hydrophobic alkyl chains, necessary for acquiring a stable Langmuir–Blodgett monolayer, are not shown in Fig. 1, and their contribution to the local-field effect is neglected.

We now proceed by presenting the details of a calculation of the second-harmonic intensity in monolayers.

The second-order nonlinear polarization component induced at site n is

$$p_i^n(2\omega) = \chi^{(2)^n}_{ijk} : E^n_{\mathrm{loc},j}(\omega)E^n_{\mathrm{loc},k}(\omega), \quad (8)$$

where the superscript n refers to the particular molecule at site n. The direction and magnitude of the microscopic local field at site n are determined by both the orientation of and the distance between neighboring molecules. On the other hand, the Cartesian components of the microscopic hyperpolarizability $\chi^{(2)^n}_{ijk}$ (in the laboratory frame) only depend on the orientation of a particular molecule at site n. We therefore may write for the average induced polarization at frequency 2ω

$$P_i(2\omega) = N_s\langle p_i^n(2\omega)\rangle = N_s\langle \chi^{(2)^n}_{ijk}\rangle : \langle E^n_{\mathrm{loc},j}(\omega)E^n_{\mathrm{loc},k}(\omega)\rangle \quad (9a)$$
$$= \chi^{(2)}_{ijk} : \langle E^n_{\mathrm{loc},j}(\omega)E^n_{\mathrm{loc},k}(\omega)\rangle, \quad (9b)$$

where $N_s\langle \chi^{(2)}_{ijk}\rangle \equiv \chi^{(2)}_{ijk}$ is given below, N_s is the surface density, and the brackets denote averaging over all sites n.

The linear and second-order susceptibility tensor elements of the isotropic monolayer just described, can easily be calculated. Averaging over all sites n implies averaging over ϕ and leaves only two independent nonvanishing components for $\chi^{(1)}$ and $\chi^{(2)}$

$$\chi^{(1)}_{xx} = \chi^{(1)}_{yy} = 1/2N_s \sin^2\psi\alpha_{\xi\xi}, \quad (10a)$$

$$\chi^{(1)}_{zz} = N_s \cos^2\psi\alpha_{\xi\xi}, \quad (10b)$$

$$\chi^{(2)}_{zxx} = \chi^{(2)}_{zyy} = 1/2N_s \sin^2\psi\cos\psi\beta_{\xi\xi\xi}, \quad (10c)$$

$$\chi^{(2)}_{zzz} = N_s \cos^3\psi\beta_{\xi\xi\xi}. \quad (10d)$$

Here $\alpha_{\xi\xi}$ is the dominant component of the molecular linear polarizability, and $\beta_{\xi\xi\xi}$ the dominant component of the molecular second-order polarizability.

From Eqs. (10) it is clear that in the absence of local-field corrections, due to interaction between the molecules in the layer, $\chi^{(1)}$ and $\chi^{(2)}$ are linear functions of surface density. Note that the off-diagonal elements of $\chi^{(1)}$ vanish in this particular coordinate system, implying that the net dipolar-reaction field is parallel to the inducing field.

In the calculation of the induced polarization $P_i(2\omega)$ [Eq. (9)] the average of the product of the fundamental field components $\langle E^n_{\mathrm{loc},j}(\omega)E^n_{\mathrm{loc},k}(\omega)\rangle$ is required. The product of off-diagonal elements of the microscopic *linear* susceptibility $\mathbf{R}\alpha\mathbf{R}^{-1}$ contained in this term does not vanish, as would be the case if $\langle E^n_{\mathrm{loc},j}(\omega)E^n_{\mathrm{loc},k}(\omega)\rangle$ were to be factored into the product $\langle E^n_{\mathrm{loc},j}(\omega)\rangle\langle E^n_{\mathrm{loc},k}(\omega)\rangle$. As will be shown later, the contributions due to the off-diagonal elements of $\mathbf{R}\alpha\mathbf{R}^{-1}$ cannot be neglected at high surface densities.

In evaluating the second-harmonic intensity from the induced polarization $P_i(2\omega)$ of Eq. (9), the local field at this frequency also needs to be considered. The microscopic local field at the harmonic frequency can be calculated by considering the monolayer as a system of dipoles, radiating at frequency 2ω. This local field is independent of the way the dipoles originally are induced. Averaging over all sites n can therefore be separated from the averaging procedures at the fundamental frequency ω.

An analytical expression for the local field cannot be obtained in this model due to a random angle ϕ. The local field in the isotropic monolayer was calculated using the Monte Carlo technique as follows. All molecules were placed on a lattice randomly with respect to ϕ, but with a fixed tilt angles ψ. A lattice of $30\times30=900$ sites was used. Density variations were simulated by incomplete padding of this lattice. In order to avoid errors in the calculation of the reaction field for dipoles close to the edges of the central dipole lattice, the partially occupied lattice was surrounded with identical lattices. Clearly, the calculation can be considered reliable only if the central lattice is taken large enough. A size of about one thousand lattice points was found to be sufficiently large. The spatial extension of this central lattice is still much less than the wavelength, which justifies the neglect of retardation. The local-field components at each site n of the central lattice were calculated iteratively until convergence was obtained. All field components thus obtained were stored to be used for calculation of an average value afterwards. The above procedure was repeated fifty times whereby each time the central lattice was filled up in a random manner. The final values

of the local-field components were obtained from an average over these fifty runs and had reached their convergent values at this point.

The limitations of the above approach should also be mentioned. The local-field corrections are only calculated through the linear polarizability, neglecting higher order contributions. Simply, the near field of the induced dipoles is used, neglecting the imaginary part,[13,34] and therefore disregarding the self field of the dipole.[33] Furthermore $\alpha_{\xi\xi}$ is assumed to be real. This is a reasonable assumption for the off-resonance fundamental frequency ω, but questionable for the preresonant harmonic frequency 2ω. A further restriction is the use of point dipoles in the calculation of the local field. The dimensions of the induced dipoles, however, are of the same magnitude as the distances between the dipoles.

Despite these limitations, the attractive feature of the above approach is that only one free (scaling) parameter is used in the calculations. This will be shown in Sec. IV.

D. Numerical results

The effect of the dipolar reaction field on the macroscopic polarization $P_z(2\omega)$, induced through $\chi^{(2)}_{zyy}$, was calculated for different tilt angles.

In case of the crystal model the induced macroscopic polarization $P_z(2\omega)$ is assumed to be,[2]

$$P_z(2\omega) = i(4\pi\omega/c)\tan\theta L_{zz}(2\omega)\ell_{zz}(2\omega)1/2N_s\sin^2\psi \times\cos\psi\beta_{\xi\xi\xi}L^2_{yy}(\omega)\ell^2_{yy}(\omega)E_{0y}(\omega)E_{0y}(\omega), \tag{11}$$

where θ is the angle of incidence, and ϕ was taken to be 45°. In the crystal model other components of $\chi^{(2)}$ exist, which are neglected in Eq. (11). There is no *a priori* justification in neglecting these components, but it will be seen that Eq. (11) does predict qualitatively the correct behavior.

The value of $P_z(2\omega)$ as a function of surface density is shown in Fig. 2. Note that in general $P_z(2\omega)$ is a nonlinear function of surface density. Note also that the nonlinear behavior of $P_z(2\omega)$ with surface density depends on the tilt angle ψ. For instance, in the case of flat lying dye molecules $P_z(2\omega)$ continues to increase in a nonlinear fashion with increasing surface coverage (see Fig. 2, for instance $\psi = 80°$), while in case of more erect standing dye molecules $P_z(2\omega)$ levels off (see Fig. 2, for instance $\psi = 10°$).

For tilt angles around 50° the dependence of $P_z(2\omega)$ on surface density is rather linear. Near the magic tilt angle the local-field factors are substantially different from unity, but it so happens that the product of the local-field factors $\ell_{zz}(2\omega)\ell^2_{yy}(\omega)$ in Eq. (11) is about one.

The behavior of $P_z(2\omega)$ as a function of the surface density is also calculated using the isotropic monolayer model. Qualitatively, the shape of $P_z(2\omega)$ as a function of surface density at a given tilt angle is similar to that predicted by the crystal model. However, pronounced differences appear at higher surface densities. Examples are given in Figs. 3–5. In Fig. 3 we plot $P_z(2\omega)$ according to the two models for a tilt angle of 10°. Using the isotropic monolayer model the amplitude of $P_z(2\omega)$ (solid line) starts to level off at lower surface densities than predicted by the crystal model (dashed line). In other words, the isotropic monolayer model yields a more pronounced deviation from linear dependence on surface density than the crystal model. The behavior of $P_z(2\omega)$ in case of a tilt angle close to the magic angle is shown in Fig. 4. Again the behavior of $P_z(2\omega)$ in either model is qualitatively the same. In case of a tilt angle larger than 40° (Fig. 5) the isotropic monolayer model predicts a steeper rise of $P_z(2\omega)$ as a function of surface density than the crystal model does. Here the calculated value of $P_z(2\omega)$ exceeds the value of the crystal model by a factor of 2 at surface densities around 3×10^{14} cm^{-2}.

It is of interest to ascertain whether in the calculations of the local-field factors according to the isotropic monolayer model the dominant contributions stem from density variations, or from the proper evaluation of the product $\langle E^n_{\mathrm{loc},j}(\omega)E^n_{\mathrm{loc},k}(\omega)\rangle$. The factorization of the fundamental field components $\langle E^n_{\mathrm{loc},j}(\omega)E^n_{\mathrm{loc},k}(\omega)\rangle$ into $\langle E^n_{\mathrm{loc},j}(\omega)\rangle\langle E^n_{\mathrm{loc},k}(\omega)\rangle$ essentially means disregarding the off-diagonal components of the linear microscopic polarizability tensor $\mathbf{R}\boldsymbol{\alpha}\mathbf{R}^{-1}$. On factorization, the off-diagonal components of $\mathbf{R}\boldsymbol{\alpha}\mathbf{R}^{-1}$ average out. In Figs. 3–5 the dash-dotted line is the result of setting $\langle E^n_{\mathrm{loc},j}(\omega)E^n_{\mathrm{loc},k}(\omega)\rangle$ to $\langle E^n_{\mathrm{loc},j}(\omega)\rangle\langle E^n_{\mathrm{loc},k}(\omega)\rangle$. From these calculations it is seen that factorization is only allowed for tilt angles close to 10°.

Summarizing: large differences (up to 100%) exist in the calculation of the local-field effects for the isotropic monolayer model compared to the crystal model. Both models, however, show qualitatively the same dependence on surface density. The nonlinear polarization in the isotropic monolayer model shows often a more pronounced deviation from a linear dependence on surface density than the crystal model. In general, local-field corrections are more pronounced in the isotropic monolayer model than in the crystal model. The effect of the nondiagonal terms in the Cartesian polarizability tensor is small when the tilt angle is close to zero.

III. EXPERIMENT

The optical nonlinear molecules used in this work are 4-(4-didecylaminostyryl)-*N*-methylpyridiniumiodide (I, see also Fig. 6) and *S*-4-(4-(1-pyrrolidine-3-ol-palmitate)phenylazo)-3-nitrobenzoïc-acid (II, Fig. 6). Dye I was purchased from Molecular Probes, Inc., and used without further purification. The synthesis of dye II will be published elsewhere.[42]

Preparation and deposition of the monolayers was established with a commercially available trough (Lauda Langmuir Balance). The Langmuir–Blodgett monolayers were deposited on Corning 7059 glass microscope slides. These substrates were cleaned in chromic acid (at least 16 h, 20 °C), and rinsed ultrasonically with milli-*Q* water, acetone, chloroform, and hexane.

A specific surface density of either dye I or II was obtained by dissolving known amounts of dye and arachidic acid (Fluka AG) in chloroform. The 10^{-3} M chloroform solution was spread onto an aqueous subphase.

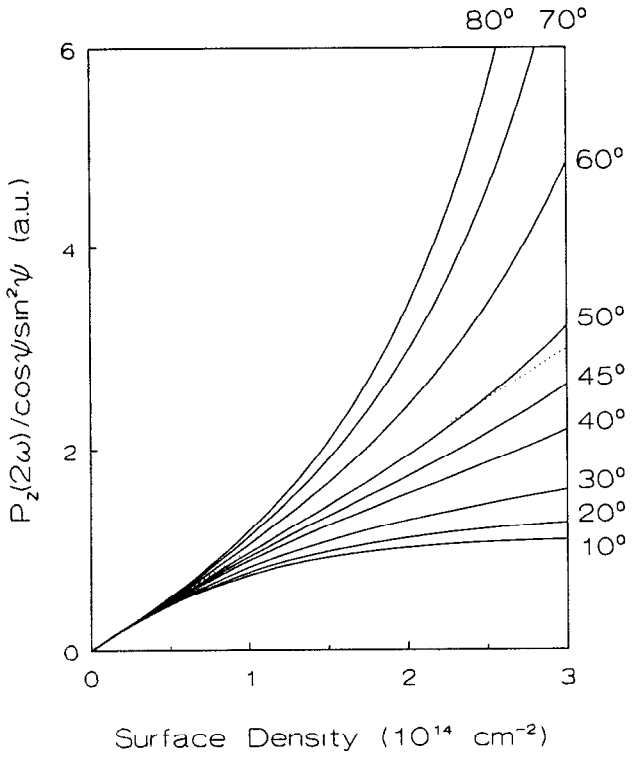

FIG. 2. Normalized values of $P_z(2\omega)$ calculated according to Eq. (11) as a function of surface density. The different traces are labeled by the tilt angles of the dye units with respect to the surface normal. The dotted line denotes the (linear) behavior in case local fields are neglected. A linear polarizability of 40 Å^3 was used in the calculations.

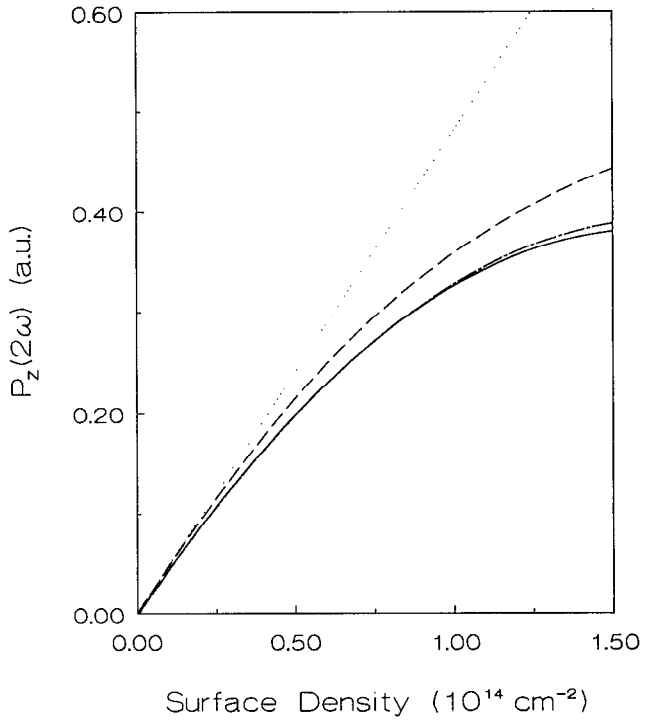

FIG. 3. Calculated values of $P_z(2\omega)$ according to the isotropic monolayer model (solid line) and the crystal model (dashed line), for a tilt angle of 10°. The dash-dotted line is the result according to the isotropic monolayer model in case the off-diagonal components of the microscopic linear polarizability are neglected. The linear behavior (dotted line) is the result of disregarding the microscopic local field. A linear polarizability of 40 Å^3 was used in the calculations.

In case of dye I the subphase contained 10^{-2} M potassium iodide, the pH was about 5.8, and the temperature 19 ± 1 °C. The resulting monolayers were compressed and stabilized at a pressure of 10 mN/m, and were deposited at this pressure by withdrawal of the hydrophilic substrate from the subphase at a rate of 4 mm/min. The dye is chemically unstable, and therefore sample preparation and handling were done in the dark, and all measurements were performed within one hour after preparation. The number of molecules per surface unit was determined from the compression isotherm, taken at a rate of 5 Å^2 per molecule per minute.

The preparation of monolayers of dye II will be published elsewhere.[43] A specific surface density of dye II was obtained in the same fashion as for dye I. The dye system is very stable, and optical measurements performed immediately or two weeks after preparation of the monolayer gave identical results.

Prior to any measurements we removed the monolayer at the backside of the substrate by wiping with lens tissues soaked in acetone and in chloroform. This in order to prevent interference between signals arising from monolayers at the front and backside of the substrate.

In the second-harmonic-generation experiment we used the linearly polarized fundamental output (1064 nm) of a Q-switched Nd^{3+}:YAG laser (Molectron Corporation). The polarization of the fundamental beam could be rotated by means of a halve-wave plate. The fundamental beam was directed onto the sample with an angle of incidence of 45°. The frequency doubled light (532 nm) was detected in reflection by a photomultiplier. Reflections from the backside of the substrate were spatially separated from front side reflections by pasting the backside of the substrate with index-matching oil to a thick piece of glass. Separation of the harmonic from the fundamental beam was accomplished by a Pellin–Broca prism and suitable color filters. The polarization direction of the second-harmonic beam was determined with a sheet polarizer (Melles–Griot). Signal sampling, averaging, and recording took place with a boxcar (Princeton Applied Research, model 162) and computer. The signal was divided by the reference signal from a KH_2PO_4 (KDP) doubling crystal. With the pulse energies used (1.5–5 mJ), the nonlinear contribution of the glass substrate covered with a monolayer of arachidic acid was below the detection limit.

The size of the error bars indicated in Figs. 11–13 is determined mainly by statistical noise in the experimental setup, due to amongst others laser amplitude fluctuations.

The absorption spectra of the monolayers were measured on a Pye Unicam SP8-200 UV/VIS spectrophotometer. Absorption spectra of the charge-transfer transition of the dye monolayers were also measured as a function of the angle of incidence. In these measurements we used a collimated polarized beam from a tungsten lamp. A double-array optical multichannel analyzer (Princeton Instru-

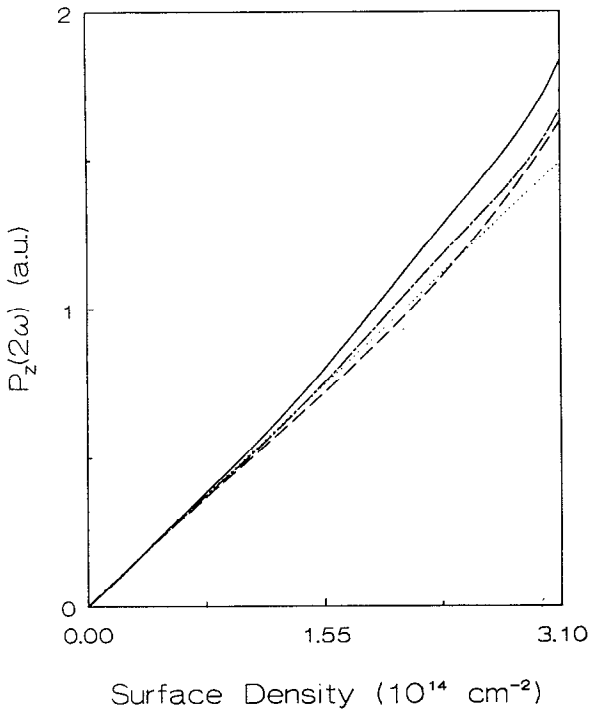

FIG. 4. Calculated values of $P_z(2\omega)$ according to the isotropic monolayer model (solid line) and the crystal model (dashed line), for a tilt angle of 50°. The dash-dotted line is the result according to the isotropic monolayer model in case the off-diagonal components of the microscopic linear polarizability are neglected. The linear behavior (dotted line) is the result of disregarding the microscopic local field. A linear polarizability of 40 Å^3 was used in the calculations.

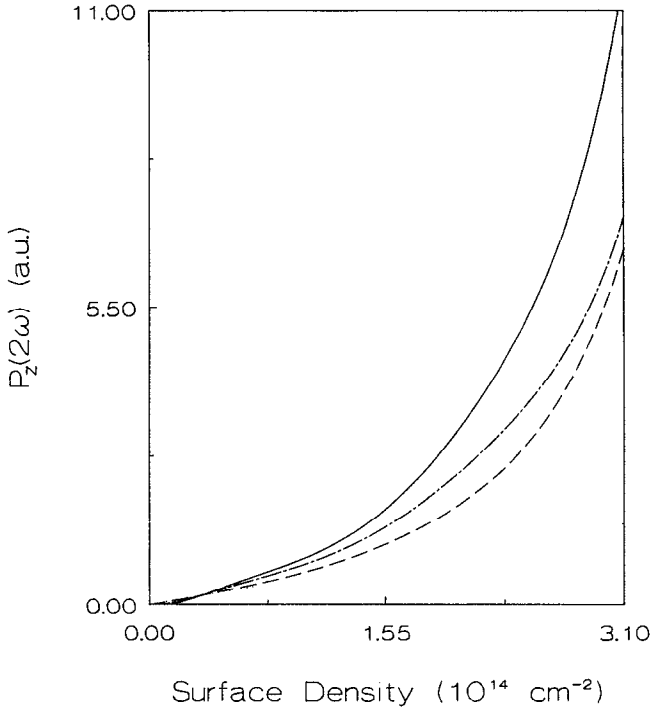

FIG. 5. Calculated values of $P_z(2\omega)$ according to the isotropic monolayer model (solid line) and the crystal model (dashed line), for a tilt angle of 80°. The dash-dotted line is the result according to the isotropic monolayer model in case the off-diagonal components of the microscopic linear polarizability are neglected. The linear behavior (dotted line) is the result of disregarding the microscopic local field. A linear polarizability of 40 Å^3 was used in the calculations.

ments, Inc.) was used to record the absorption spectra. In order to obtain the internal absorbance of the monolayer the total absorption has to be corrected for reflection losses at every angle of incidence. Reflection losses were measured using a reference object consisting of a glass slide covered with a monolayer of pure arachidic acid.

The numerical calculations described in Sec. II were done on a Convex 230 minisupercomputer.

IV. EXPERIMENTAL RESULTS

A. General aspects

The second-harmonic intensity was measured in reflection with an incident angle of 45°. For both dye systems the following set of second-harmonic intensities were measured: $I_{pp}(2\omega)$, $I_{ps}(2\omega)$, $I_{qp}(2\omega)$, $I_{qs}(2\omega)$, $I_{sp}(2\omega)$, and $I_{ss}(2\omega)$. Here, the first and second subscript label the input and output polarization directions, respectively. p and s refer, respectively, to the polarization directions parallel and perpendicular to the plane of incoming and outgoing beams (the $\hat{x}$-$\hat{z}$ plane). The polarization direction inbetween s and p is denoted as q, i.e., 45° with respect to the plane of incidence.

A typical result obtained for both dye systems is shown in Fig. 7. $I_{ss}(2\omega)$ and $I_{ps}(2\omega)$ are found to be two orders or magnitude smaller than the other polarization combinations, confirming the uniaxial symmetry of the system (Fig. 1).[2,44] The uniaxiality of the system derives further support from polarized absorption measurements.

For both dye systems the second-harmonic intensities $I_{pp}(2\omega)$, $I_{ps}(2\omega)$, $I_{qp}(2\omega)$, $I_{qs}(2\omega)$, $I_{sp}(2\omega)$, and $I_{ss}(2\omega)$ were measured as a function of density of the dye mole-

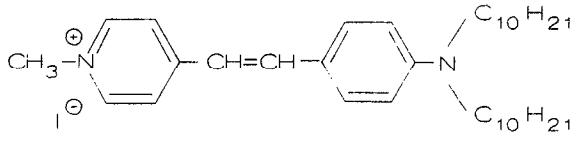

I

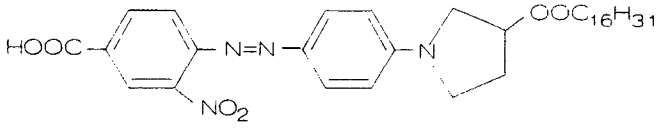

II

FIG. 6. Chemical formulas of the studied dye molecules.

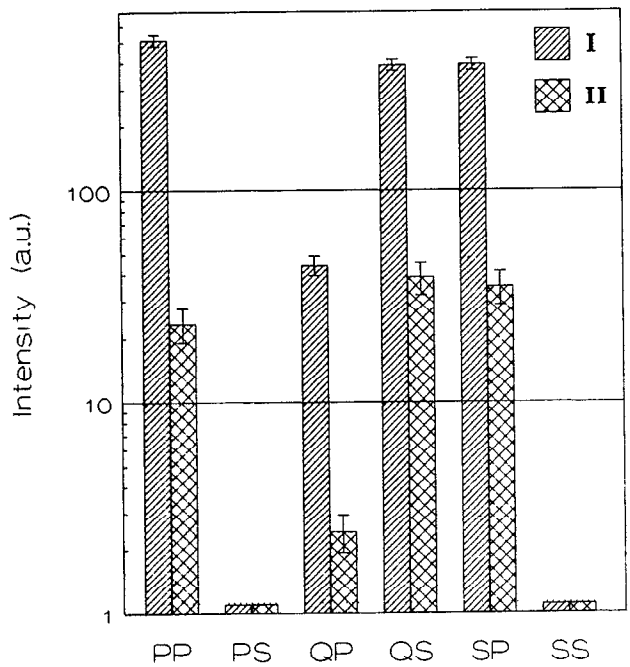

FIG. 7. Histogram of the observed p- and s-polarized second-harmonic intensities as measured in reflection for different polarization directions of the fundamental beam. Full monolayer coverage signal strengths for dyes I and II are given. The dotted line indicates the detection limit.

cules. Figure 11 displays the observed relation for I_{sp} in the case of dye system I. Clearly, $\sqrt{I_{sp}}$ is not linear in surface density. It is tempting to interpret this behavior in terms of a local-field effect, but in order to draw this conclusion two other effects that could influence second-harmonic generation I_{sp} have to be ruled out. First, aggregation could occur at high surface densities. This possibility is considered in the next section. Second, the tilt angle of the dye units might change as a function of surface density. An investigation concerning this problem is described in the Sec. IV C. After having addressed these problems and concluded that neither effect plays a role in the monolayers studied, we continue in Sec. IV D with a discussion of the density dependence of the second-harmonic intensity.

B. Aggregation

We recall that $I_{ss}(2\omega)$ and $I_{ps}(2\omega)$ were found to be 2 orders of magnitude smaller than the other second-harmonic intensities. This fact indicates that the samples are macroscopically isotropic with respect to the substrate plane and that aggregate formation is highly unlikely.[45] The near equality of the intensities of $I_{qs}(2\omega)$ and $I_{sp}(2\omega)$ further supports this assumption.[46] Further evidence for the absence of aggregation stems from the density dependence of the absorption spectra of both dyes. Figures 8 and 9 display these spectra for low surface coverage (dashed line) and maximum surface density (solid line). It is clear that the spectra show no broadening and/or shift of the charge-transfer band in the regime of densities studied. These findings strongly suggests that the optical excitations in these films can effectively be considered

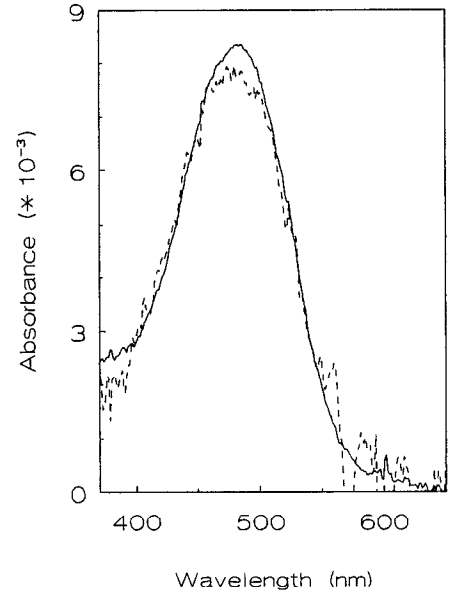

FIG. 8. Absorption spectra of dye I at full monolayer coverage (1.5055×10^{14} cm^{-2}, solid line) and at low surface density (0.36×10^{14} cm^{-2}, dashed line). The absorbance scale corresponds to the full monolayer case.

as localized, implying that the local inhomogeneity exceeds by far the dipolar coupling between the sites. The assumption of localized excitations in these Langmuir–Blodgett films is basic to the local-field approach taken in this paper. It should be noted, however, that for substrates that were not cleaned immediately prior to use, a blueshift of the absorption band can be observed, which is indicative of H-aggregate formation.

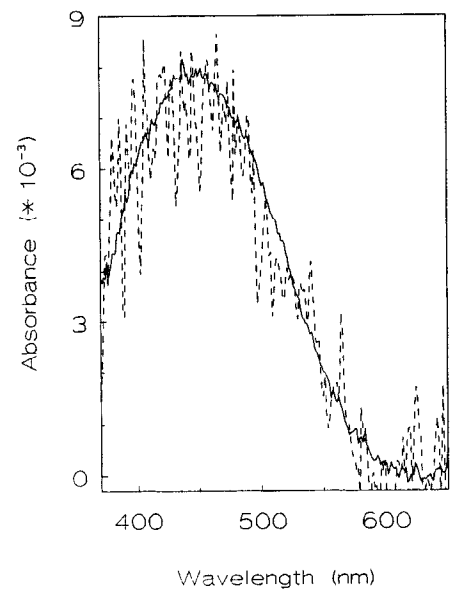

FIG. 9. Absorption spectra of dye II at full monolayer coverage (3.03×10^{14} cm^{-2}, solid line) and at low surface density (0.41×10^{14} cm^{-2}, dashed line). The absorbance scale corresponds to the full monolayer case.

The change in surface acidity resulting from dilution of the dye molecules with arachidic acid has no effect on the absorption spectrum, as expected for the molecules under study.[44,47] Its effect on the nonlinear optical properties can therefore be neglected.

C. The tilt angle

Knowledge of the tilt angle ψ of the dye unit is essential to predicting the second-harmonic intensity as a function of the surface density. In principle the tilt angle ψ can be determined by second-harmonic generation. However, in case local-field corrections are important, this calculation is extremely laborious for the following reasons. First, the tilt angle itself is an important parameter in the calculation of macroscopic field corrections of Eq. (1). The dielectric constant of the monolayer ϵ' in Eq. (1c) is a rather critical parameter,[46] and depends on the tilt angle through Eq. (10a).[45] Small modifications of the dielectric constant lead to substantial changes in the obtained tilt angle.[46] Second, also the microscopic local-field correction is rather sensitive to the tilt angle, as follows from the numerical calculations of Sec. II (cf. Figs. 2–5). The microscopic local field will also influence the dielectric constant of the monolayer. Third, the optical nonlinearities often allow two possible solutions for the tilt angle ψ and additional information is needed to make a choice.

Clearly, it would be extremely valuable if another independent method could give an initial estimate of the tilt angle. For our systems a polarization-dependent study of the optical density turns out to be extremely useful. The anisotropy of the absorbance stems from the fact that the transition dipole moment of the charge-transfer transition is directed along the ξ axis. The derivation of the relevant formula for the angular-dependent absorption is given in the Appendix. In calculating the tilt angle from linear spectroscopy the dielectric constant of the monolayer is also requested, but its precise value is not so important to the outcome. In case no spectral shifts occur, the microscopic local field has no influence on the optical density.[48]

For dyes I and II the tilt angles were determined by the optical-density method, and were found to be 80°(±5) and 50°(±2), respectively. A tilt angle of 80° for dye I agrees well with a report[44,49] for a similar molecule. For dye II a calculation of ψ indicates that the tilt angle is close to the magic angle (54.7°), making a calculation of ψ virtually independent of the choice of the dielectric constant ϵ' of the monolayer. For a magic tilt angle the optical density is independent of the angle of incidence on the substrate.

From angular-dependent absorption measurements it was concluded that the tilt angle is independent of the surface density. Confirmation of this fact comes from a plot of the optical density vs surface density. The results are shown in Fig. 10. For both dyes a linear behavior is found, indicating that the respective tilt angles of the dye units do not change with surface coverage in the density regime studied.

The tilt angles determined in this way are in complete agreement with the ones obtained from a second-harmonic generation experiment, once the local-field corrections are incorporated. For the calculation of ψ from SHG data, the dielectric constants of the monolayer are important. The values $\epsilon'_{zz}(2\omega) = 2.66$ and $\epsilon'_{zz}(\omega) = 2.50$ were used for a monolayer of dye II.[50] The ratio $\epsilon'(2\omega)/\epsilon'(\omega)$ is in excellent agreement with the ratio obtained from $I_{qs}(2\omega)$ and $I_{sp}(2\omega)$.[46] The z component of ϵ' has been used in the calculations.[5] For dye I the dielectric constant ϵ'_{zz} was supposed to be close to 1, because of the large tilt angle ψ. The tilt angle deduced from SHG data is not very sensitive to the microscopic local-field corrections (±5°). We found this to be true for both the crystal model as well as the isotropic monolayer model. In case of dyes I(II) the tilt angles deduced from SHG changes 5°(2°) using the microscopic local-field correction factors. The smallest differences ($\approx$2°) are found for tilt angles close to 50°. These findings corroborate the results of Heinz *et al.*[41] who found that tilt angles hardly depend on microscopic local-field corrections.

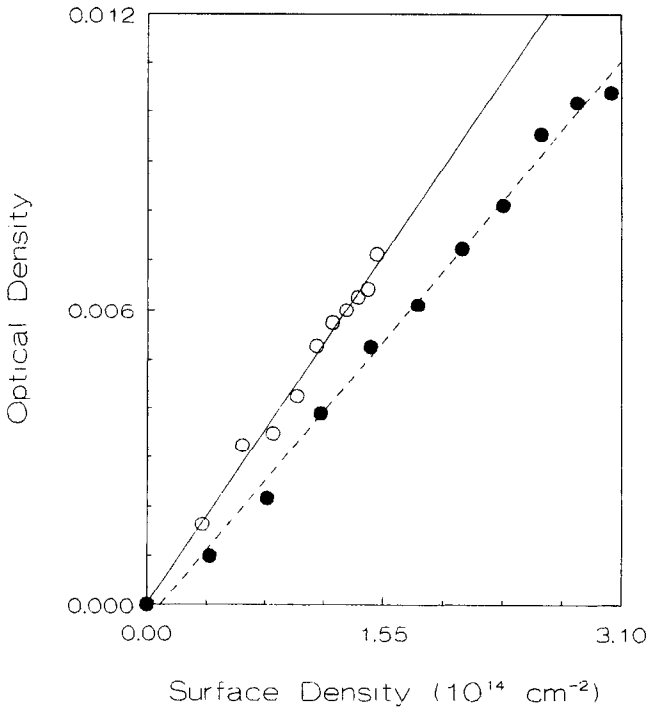

FIG. 10. Measurement of the optical density for dye I (open circles) and dye II (closed circles) as a function of surface density, measured at a perpendicular angle of incidence. The straight lines are least square fits to the measurements.

The difference in tilt angles of the chromophores also manifests itself in the maximum surface density that can be reached, before the monolayer collapses or aggregation occurs. For almost flat lying dye molecules, like I, lower surface densities (1.5055×10^{14} cm^{-2}) can be reached than for the more erect ones like II (3.03×10^{14} cm^{-2}).

In summary the tilt angles deduced from absorption and second-harmonic generation (SHG) measurements are in excellent agreement with one another. The advantage of the absorption method as compared to the SHG measurements is that the deduced tilt angle is not very sensitive to the value of the monolayer dielectric constant.

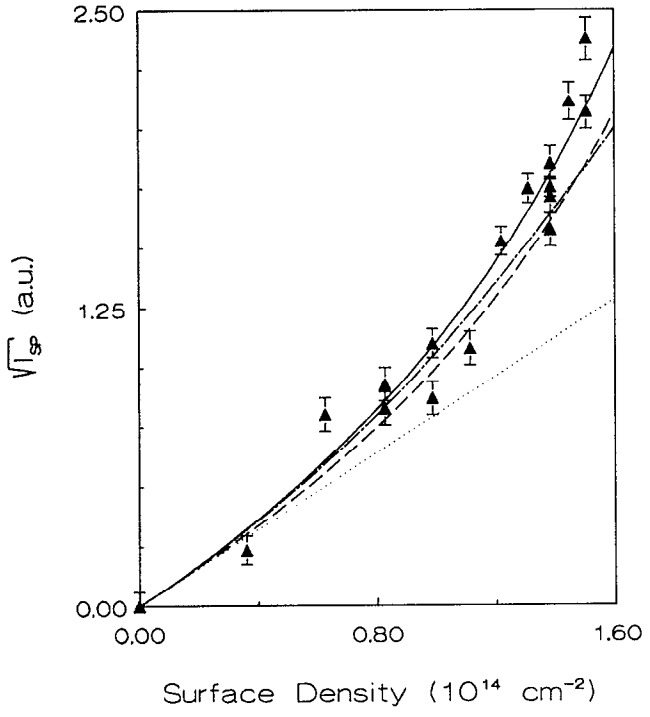

FIG. 11. Measured values of $\sqrt{I_{sp}}$ for monolayers of dye I as a function of surface density (triangular points). Also shown are the results of the calculations according to the isotropic monolayer model (solid line), the crystal model (dashed line), and in case the off-diagonal components of the linear microscopic polarizability are neglected (dash-dotted line). The dotted line is the result of disregarding the microscopic local field. In the calculations a linear polarizability of 50 Å^3 was used.

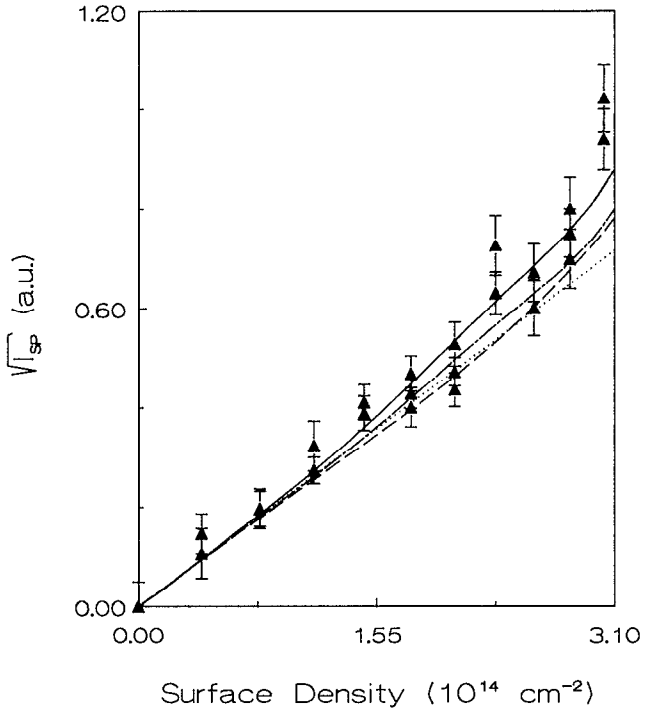

FIG. 12. Measured values of $\sqrt{I_{sp}}$ for monolayers of dye II as a function of surface density (triangular points). Also shown are the results of the calculations according to the isotropic monolayer model (solid line), the crystal model (dashed line), and in case the off-diagonal components of the linear microscopic polarizability are neglected (dash-dotted line). The dotted line is the result of disregarding the microscopic local field. In the calculations a linear polarizability of 40 Å^3 was used.

D. Microscopic local-fields: Dependence of $\chi^{(2)}$ on surface density

For dye I ($\psi = 80°$) the measured and calculated relation between $\sqrt{I_{sp}}$ and increasing surface density is shown in Fig. 11. Scatter in the data is ascribed to the chemical instability of the dye unit. Note from Eq. (11) that $\sqrt{I_{sp}}$ is proportional to the amplitude of $P_z(2\omega)$. The observed second-harmonic efficiency (triangular points) increases in a nonlinear fashion with surface density. As argued in preceding sections, no hints of aggregation occur, while also the tilt angle is independent of the surface density. We therefore conclude that this nonlinear behavior is due to local-field effects. The result of the Monte Carlo calculations based on the isotropic monolayer model (solid line) is in excellent agreement with the measurements. The crystal-model calculation (dashed line) also yields a good description except for high surface densities. Analogous results have been found for $\sqrt{I_{pp}}$.

We emphasize that only one free parameter, the molecular hyperpolarizability $\beta_{\xi\xi\xi}$, enters into the calculation of the local field, the rest of the parameters are either measured or known. For dye I a lattice constant of 8.15 Å was calculated from the compression isotherm. For the molecular polarizability $\alpha_{\xi\xi}$ a value of 50 Å^3 was taken at the harmonic as well as at fundamental frequency.[51] The dispersion in $\alpha_{\xi\xi}$ is neglected, because of the fact that the results of the calculations are not very critical to the value of the linear polarizability.

The value of the molecular hyperpolarizability $\beta_{\xi\xi\xi}$, as inferred from the measured $\chi^{(2)}_{zyy}$, differs (at full coverage) by a factor 2 from the local-field corrected value (dotted line, Fig. 11). The microscopic local field can be the reason for the exceptionally large $\chi^{(2)}$ measured for monolayers of dye I.[17,44]

For dye II a tilt angle ψ of 50° was found. The experimentally observed behavior of $\sqrt{I_{sp}}$ for dye II as a function of surface density is given in Fig. 12. Indeed, as might be expected for a tilt angle of 50° (see Fig. 2) a rather linear dependence of $\sqrt{I_{sp}}$ on surface density is observed. The isotropic monolayer model, at high surface densities, still yields a better fit (solid line), than provided by the crystal model (dashed line). The lattice constant for this dye was determined to be 5.74 Å, and the molecular polarizability was taken to be 40 Å^3.[52,53]

The small deviation from linear behavior might suggest that the local-field corrections are of minor importance in this case.[29,54] The linearlike behavior, however, is due to the fact that near the magic tilt angle a cancellation of local-field correction factors occurs. The field along the y axis (parallel to the substrate) is about 1.4 times the applied field, while the field along $\hat{z}$ (i.e., perpendicular to the substrate) is calculated to be about 0.5 times the applied field.

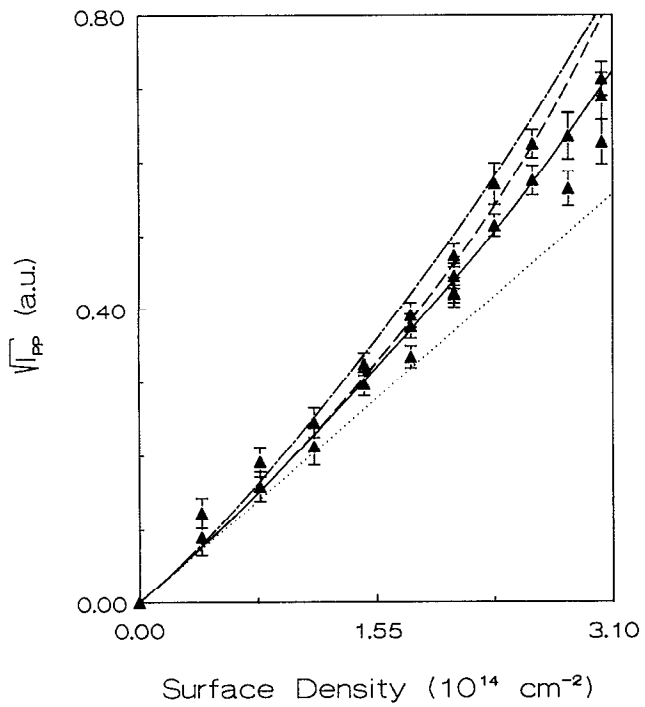

FIG. 13. Measured values of $\sqrt{I_{pp}}$ for monolayers of dye II as a function of surface density (triangular points). Also shown are the results of the calculations according to the isotropic monolayer model (solid line), the crystal model (dashed line), and in case the off-diagonal components of the linear microscopic polarizability are neglected (dash-dotted line). The dotted line is the result of disregarding the microscopic local field. In the calculations a linear polarizability of 40 Å^3 was used.

For dye II the measured and calculated behavior of $\sqrt{I_{pp}}$ with surface density are given in Fig. 13. For this polarization combination the fundamental and second-harmonic beams are both polarized parallel to the plane of incidence. The fundamental field can be decomposed into a parallel $[E_x(\omega)]$ and perpendicular $[E_z(\omega)]$ electric field component to the substrate surface. The emitted second-harmonic signal is then proportional to the difference between the two nonlinearly induced polarizations $P_x(2\omega)$ and $P_z(2\omega)$. The off-diagonal components of the *linear* susceptibility tensor $\mathbf{R}\alpha\mathbf{R}^{-1}$ [Eq. (9)] also yield a contribution to the fundamental field along the y axis $[\langle E^n_{\mathrm{loc},y}(\omega) E^n_{\mathrm{loc},y}(\omega)\rangle]$. This latter quantity contributes through $\chi^{(2)}_{zyy}$ to the second-harmonic polarization $P_z(2\omega)$. This additional contribution to $P_z(2\omega)$ reduces the difference between $P_x(2\omega)$ and $P_z(2\omega)$ and therefore leads to a measurable decrease of $\sqrt{I_{pp}}$ at high surface densities (solid line). In case the off-diagonal elements of $\mathbf{R}\alpha\mathbf{R}^{-1}$ are neglected (dash-dotted line), a steeper increase of $\sqrt{I_{pp}}$ is calculated. The result of the computations according to the crystal model are plotted as the dashed line. It is clear that in this case the contribution of the off-diagonal terms of $\mathbf{R}\alpha\mathbf{R}^{-1}$ cannot be disregarded at higher surface densities.

V. DISCUSSION AND CONCLUSIONS

In this paper we showed that a Monte Carlo calculation of the local field in a monolayer of rod-shaped chromophores yields good agreement between theory and experiment in second-harmonic generation experiments. We found that Monte Carlo calculations of the local field can differ up to a factor of 2 from what is obtained by using a crystal model. The qualitative behavior of $\chi^{(2)}$ vs surface density in both models, however, is the same. These results are clearly relevant when SHG is used in a determination of the molecular hyperpolarizability $\beta_{\xi\xi\xi}$. The values reported in the literature for $\beta_{\xi\xi\xi}$ have often been obtained from Langmuir–Blodgett monolayers at maximum surface density using the three-dimensional Lorentz–Lorenz expressions for the local field, or by using local-field corrections based on the crystal model. Our work shows that by this approach the value of $\beta_{\xi\xi\xi}$ can be overestimated or underestimated depending on the spatial orientation of the optical nonlinearity.

In the systems studied no additional broadening of the experimental spectra at high surface density could be observed within experimental accuracy (about 200 cm^{-1}). However, a broadening of approximately 1500 cm^{-1} due to dipolar interactions is calculated for a simple two-level system.[15] The absence of such a large broadening is attributed to inhomogeneous broadening of the optical transition, which *at resonance* considerably reduces the dipolar coupling. Off-resonance however, the molecular polarizability may be assumed to be site independent. Hence, in our local-field calculations the effect of inhomogeneous broadening on dipolar interactions was neglected.

To calculate the microscopic local field a large number of parameters are needed: (1) the dielectric constants $\epsilon'(\omega)$, $\epsilon'(2\omega)$ of the monolayer at the fundamental and the second-harmonic frequency, (2) the polarizability $\alpha_{\xi\xi}$ at ω and 2ω, (3) the tilt angle of the dye molecules, (4) the mean distance between the dye units, and (5) the absolute value of $\beta_{\xi\xi\xi}$. To complicate matters further, both ϵ' and α can be complex. In addition, ϵ' will depend on the surface density, while also the tilt angle may be a function of surface density. In this paper the number of free parameters could successfully be restricted to one, namely the absolute value of the molecular hyperpolarizability $\beta_{\xi\xi\xi}$. The value of the other parameters were known or could be determined independently. Despite these complications our Monte Carlo calculations reproduce extremely well the experimentally observed behavior of the different $\chi^{(2)}$ components, justifying our approach.

ACKNOWLEDGMENTS

We thank M. A. Schoondorp and Dr. A. J. Schouten of the Polymer Chemistry Department for use of the Langmuir–Blodgett film growth facility and for sharing their knowledge with us concerning the fabrication of monolayers. We are also indebted to J. B. E. Hulshof and Professor B. L. Feringa of the Organic Chemistry Department for the synthesis and gift of dye II. We express our gratitude to F. de Haan for creating the computer programs for the Monte Carlo calculations and instrument control. The investigations were supported by the Dutch Organization for Innovative Research (IOP/PCBP) and by AKZO, Inc.

APPENDIX

The optical density of a transition is proportional to $|\mu \cdot \mathbf{E}|^2$, where μ is the transition dipole moment and $\mathbf{E}$ the electromagnetic field. The relation between the components of the transition dipole moment in the laboratory frame and the molecular frame is given by

$$\mu = \begin{pmatrix} \cos\phi \sin\psi \\ \sin\phi \sin\psi \\ \cos\psi \end{pmatrix} \mu_0. \tag{A1}$$

Here μ_0 is the transition dipole moment directed along the molecular ξ axis. The angles ψ and ϕ are shown in Fig. 1.

For a parallel-polarized light beam the electric field in the film is given by

$$\mathbf{E} = \begin{pmatrix} \cos\theta' \\ 0 \\ \sin\theta' \end{pmatrix} \mathbf{E}_0 = \begin{pmatrix} (\epsilon' - \sin^2\theta)^{1/2} \\ 0 \\ \sin\theta \end{pmatrix} \mathbf{E}_0 / \sqrt{\epsilon'}, \tag{A2}$$

where θ is the angle of incidence on the sample, θ' the angle of refraction in the monolayer, and ϵ' is the dielectric constant of the monolayer, which for simplicity is supposed to be isotropic.

The optical density for a parallel polarized light beam (OD_p) is calculated as

$$OD_p = Q(\theta)\langle(\mu \cdot \mathbf{E})^2\rangle, \tag{A3}$$

$$= \frac{Q}{\cos\theta}\{1/2 \sin^2\psi + (\cos^2\psi - 1/2 \sin^2\psi)\sin^2\theta/\epsilon'\}, \tag{A4}$$

where $\langle\ \rangle$ means averaging over ϕ. The proportionality constant $Q(\theta)$ contains, amongst others, the number of molecules in the beam, which depends on the angle of incidence θ. By varying θ, the number of absorbing molecules is changed. To correct for this effect, $Q(\theta)$ is divided by $\cos\theta$.

A plot of $OD_p \times \cos\theta$ against $\sin^2\theta$ should give a straight line. The tilt angle ψ can be determined from the ratio of the slope S and the abscissa A

$$\tan^2\psi = 2/\{(S/\epsilon' A) + 1\}, \tag{A5}$$

in which case Q is divided out. Changes in reflection losses, upon varying the angle of incidence, are corrected for by subtraction of a reference spectrum of a virgin glass slide.

[1] Y. R. Shen, Nature (London) **337**, 519 (1989).
[2] Y. R. Shen, Annu. Rev. Phys. Chem. **40**, 327 (1989).
[3] C. K. Chen, T. F. Heinz, D. Ricard, and Y. R. Shen, Phys. Rev. B **27**, 1965 (1983).
[4] G. T. Boyd, Th. Rasing, J. R. R. Leite, and Y. R. Shen, Phys. Rev. B **30**, 519 (1984).
[5] T. F. Heinz, PhD. thesis, Univ. of Calif., Berkeley, 1982.
[6] G. J. Kovacs, R. O. Loufty, P. S. Vincent, C. Jennings, and R. Aroca, Langmuir **2**, 689 (1986).
[7] T. M. Cotton, R. A. Uphaus, and D. Möbius, J. Phys. Chem. **90**, 6071 (1986).
[8] K. E. Drabe, G. Cnossen, and D. A. Wiersma, Opt. Commun. **73**, 91 (1989).
[9] K. E. Drabe, G. Cnossen, and D. A. Wiersma, Chem. Phys. Lett. **169**, 416 (1990).
[10] C. K. Carniglia, L. Mandel, and K. H. Drexhage, J. Opt. Soc. Am. **62**, 479 (1972).
[11] P. Guyot-Sionnest, Y. R. Shen, and T. F. Heinz, Appl. Phys. B **42**, 237 (1987).
[12] J. Knoester and S. Mukamel, J. Opt. Soc. Am. B **6**, 643 (1989).
[13] J. D. Jackson, *Classical Electrodynamics*, 2nd ed. (Wiley, New York, 1975).
[14] B. F. Levine and C. G. Bethea, J. Chem. Phys. **63**, 2666 (1975).
[15] J. J. Maki, M. S. Malcuit, J. E. Sipe, and R. W. Boyd, Phys. Rev. Lett. **67**, 972 (1991).
[16] H. Hsiung, G. R. Meredith, H. Vanherzeele, R. Popovitz-Biro, E. Shavit, and M. Lahav, Chem. Phys. Lett. **164**, 539 (1989).
[17] D. Lupo, W. Prass, U. Scheunemann, A. Leschewsky, H. Ringsdorf, and I. Ledoux, J. Opt. Soc. Am. B **5**, 300 (1988).
[18] F. C. Spano, S. Mukamel, Phys. Rev. A **40**, 5783 (1989); A **41**, 5243 (E) (1990).
[19] F. C. Spano and S. Mukamel, Phys. Rev. Lett. **66**, 1197 (1991).
[20] L. M. Hayden, Phys. Rev. B **38**, 3718 (1988).
[21] K. Shirota, K. Kajikawa, H. Takezoe, and A. Fukada, Jpn. J. Appl. Phys. **29**, 750 (1990).
[22] K. Kajikawa, K. Shirota, H. Takezoe, and A. Fukada, Jpn. J. Appl. Phys. **29**, 913 (1990).
[23] K. Kajikawa, H. Takezoe, and A. Fukuda, Jpn. J. Appl. Phys. **30**, 1050 (1991).
[24] J. S. Schildkraut, T. L. Penner, C. S. Willand, and A. Ulman, Opt. Lett. **13**, 134 (1988).
[25] G. Marowsky and R. Steinhoff, Opt. Lett. **13**, 707 (1988).
[26] I. R. Girling, N. A. Cade, P. V. Kolinsky, R. J. Jones, I. R. Peterson, M. M. Ahmad, D. B. Neal, M. C. Petty, G. G. Roberts, and W. J. Feast, J. Opt. Soc. Am. B **4**, 950 (1987).
[27] A. Scheelen, P. Winant, and A. Persoons, *Conjugated Polymeric Materials: Opportunities in Electronics, and Molecular Electronics*, edited by J. L. Bredas and R. R. Chance (Kluwer Academic, Dordrecht, 1990), p. 443.
[28] P. Winant, A. Scheelen, and A. Persoons, *Nonlinear Optical Effects in Organic Polymers*, edited by J. Messier *et al.* (Kluwer Academic, Dordrecht, 1989), p. 219.
[29] G. Berkovic, Th. Rasing, and Y. R. Shen, J. Opt. Soc. Am. B **4**, 945 (1987).
[30] J. Bauer, P. Jeckeln, D. Lupo, W. Prass, U. Scheunemann, R. Keosian, and G. Khanarian, *Organic Materials for Nonlinear Optics*, edited by R. A. Hann and D. Bloor (Royal Society of Chemistry, London, 1989), p. 348.
[31] A. Bagchi, R. G. Barrera, and R. Fuchs, Phys. Rev. B **25**, 7086 (1982).
[32] A. Bagchi, R. G. Barrera, and B. B. Dasgupta, Phys. Rev. Lett. **44**, 1475 (1980).
[33] D. Bedaux and N. Bloembergen, Phys. (Utrecht) **69**, 57 (1973).
[34] J. Van Kranendonk and J. E. Sipe, *Progress in Optics*, edited by E. Wolf (North–Holland, Amsterdam, 1977), Vol. 15, p. 245.
[35] P. Ye and Y. R. Shen, Phys. Rev. B **28**, 4288 (1983).
[36] W. H. de Jeu and P. Bordewijk, J. Chem. Phys. **68**, 109 (1978).
[37] M. Orrit, D. Möbius, U. Lehmann, and H. Meyer, J. Chem. Phys. **85**, 4966 (1986).
[38] H. Hoek, Dissertation, Univ. of Leiden, Leiden, 1939.
[39] F. Reiche, Ann. Phys. **50**, 1, 121 (1916).
[40] J. Topping, Proc. R. Soc. London, Ser. A **114**, 67 (1927).
[41] T. F. Heinz, H. W. K. Tom, and Y. R. Shen, Phys. Rev. A **28**, 1883 (1983).
[42] J. B. E. Hulshof, E. P. Schudde, B. L. Feringa, M. A. Schoondorp, and A. J. Schouten (to be published).
[43] M. A. Schoondorp, A. J. Schouten, J. B. E. Hulshof, and B. L. Feringa (to be published).
[44] G. Marowsky, L. F. Chi, D. Möbius, R. Steinhoff, Y. R. Shen, D. Dorsch, and B. Rieger, Chem. Phys. Lett. **147**, 420 (1988).
[45] O. A. Aktsipetrov, N. N. Akhmediev, J. M. Baranova, E. D. Mishina, and V. R. Novak, Sov. Phys. JETP **62**, 524 (1985).
[46] T. G. Zhang, C. H. Zhang, and G. K. Wong, J. Opt. Soc. Am. B **7**, 902 (1990).
[47] X. Xiao, V. Vogel, and Y. R. Shen, J. Chem. Phys. **94**, 2315 (1991).
[48] M. R. Philpott, J. Chem. Phys. **61**, 5306 (1974).
[49] R. W. J. Hollering and W. J. O. V. Teesselink, Opt. Commun. **79**, 224 (1990).
[50] N. J. Geddes, M. C. Jurich, J. D. Swalen, R. Twieg, and J. F. Rabolt, J. Chem. Phys. **94**, 1603 (1991).

[51] B. F. Levine, C. G. Bethea, E. Wasserman, and L. Leenders, J. Chem. Phys. **68**, 5042 (1978).
[52] H. Kuhn and A. Schweig, Chem. Phys. Lett. **1**, 255 (1967).
[53] G. Khanarian, A. Artigliere, R. Keosian, E. W. Choe, R. DeMartino, D. Stuetz, and C. C. Teng, Proc. SPIE. Int. Soc. Opt. Eng. **682** (Mol. Polym. Optoelectron. Mater.: Fundam. Appl.), 153 (1986).
[54] Th. Rasing, G. Berkovic, Y. R. Shen, S. G. Grubb, and M. W. Kim, Chem. Phys. Lett. **130**, 1 (1986).